

2019 NA62 Status Report to the CERN SPSC

Abstract

The status of the NA62 experiment is reported. The ongoing activities on detectors and hardware are summarised, together with a review of the data processing. The status of the $K^+ \rightarrow \pi^+ \nu \bar{\nu}$ analysis of the 2017 data set is presented and highlights of rare and forbidden decay analyses and exotic searches are also briefly discussed.



1 Introduction

The NA62 experiment collected its first data sample successfully in 2016; since then:

- the new in-flight technique to measure the branching ratio of the ultra-rare $K^+ \rightarrow \pi^+ \nu \bar{\nu}$ decay has been established and proven to work;
- the first physics result on $K^+ \rightarrow \pi^+ \nu \bar{\nu}$ based on 2016 data set was achieved in 2018 and published in early 2019 [1];
- further data samples were successfully accumulated in 2017 and 2018 data taking periods.

This NA62 2019 report to the SPSC focuses on an update of the $K^+ \rightarrow \pi^+ \nu \bar{\nu}$ analysis performed on the 2017 data set, using the same strategy as that used for the 2016 data publication.

The 2018 data taking lasted for 217 days, from April 9 to November 12 (56 days longer than in 2017). The installation of the Fixed Collimator happened during a long MD on June 18-21. Beam intensity was kept stable at 60–70% of nominal, corresponding to about $2 - 2.3 \times 10^{12}$ protons per pulse (ppp), optimised for efficient data taking conditions. Towards the end of 2018 data taking, several test runs were taken at 100% nominal beam intensity to investigate trigger and detector performance. In addition, about one week was dedicated to beam dump mode. The 2018 data taking was very successful and proceeded very smoothly, mainly due to the stable beam delivered by the SPS and the good performance of the hardware.

The analysis of 2018 data will benefit from the experience acquired from 2017 data and will focus on re-optimizing the whole strategy to improve the signal sensitivity. Important progress was made in 2018 at the software level and online/offline monitoring level, as well as in the reconstruction and processing of the data, improving the overall data quality.

The FRC of November 2018 approved the budget for 2019 and the outlook for 2020; this allows us to prepare for data taking after LS2. The limitations in the L0TP firmware, identified during the high intensity test runs in 2018, are being addressed, and we plan to take data at 100% nominal intensity when beam is back after LS2. In view of data taking at 100% nominal intensity from 2021, we are working towards reducing the random veto, further improving the TDAQ, and making the $K^+ \rightarrow \pi^+ \nu \bar{\nu}$ analysis more performant.

Thanks to a substantial analysis effort, several physics analyses are presently ongoing, spanning precision measurements, searches for lepton number and flavour violating processes, and searches for exotic long living particles.

The document is structured as follows: Sections 2 and 3 summarise the ongoing activities on the hardware and the data processing, respectively; the $K^+ \rightarrow \pi^+ \nu \bar{\nu}$ analysis on the 2017 data is described in Section 4; Sections 5 and 6 report current highlights of rare/forbidden decays and exotic searches, respectively. Finally the list of recent publications is presented in Section 7.

2 Status of the Detector and Ongoing Activities

Improvements to the radiation shielding were made prior to the 2018 data taking. The electronics racks for the KTAG, CHANTI and GTK cooling stations were equipped with additional concrete blocks to decrease the number of single event upsets (SEUs). In addition, neutron shielding (boron carbide) was added to electronics racks of the KTAG. A reduction factor greater than 10 for high-energy hadrons was achieved and the thermal neutron flux was decreased by a factor greater than 25. The boron carbide shielding alone decreased the thermal neutron flux by a factor greater than 10.

The level of the liquid krypton in the LKr detector has been stable since the summer of 2017 and there is no urgent need to top up the liquid krypton at this point. Nevertheless 400 litres of

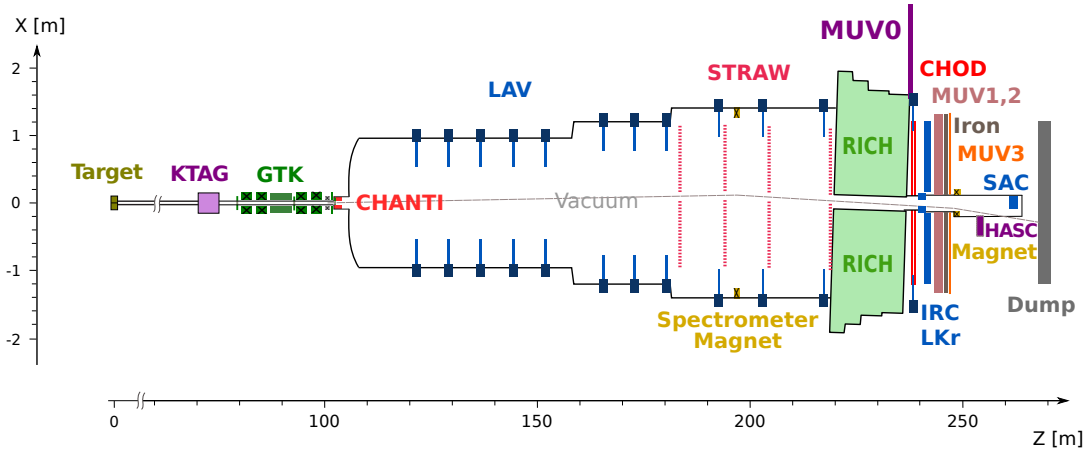


Figure 1: Layout of the NA62 experiment. KTAG: differential Cherenkov counter; GTK: Si pixel beam tracker; CHANTI: ring stations of scintillator slabs; LAV: lead glass ring calorimeters; STRAW: straw magnetic spectrometer; RICH: ring imaging Cherenkov counter; MUV0: off-acceptance plane of scintillator pads; CHOD: planes of scintillator pads and slabs; IRC: inner ring shashlik calorimeter; LKr: electromagnetic calorimeter filled with liquid krypton; MUV1,2: hadron calorimeter; MUV3: plane of scintillator pads for muon veto; HASC: near beam lead-scintillator calorimeter; SAC: small angle shashlik calorimeter.

liquid krypton were bought in 2017 and they will be added to the krypton storage dewar later in 2019. A dedicated device has been built to validate the purity of the krypton by measuring the lifetime of the drift electrons. The first tests with this new device were carried out in the summer of 2018. The first results from these measurements were not conclusive due to high noise level in the readout. In order to improve the signal-to-noise ratio it was decided to modify the front-end electronics before making a final validation in the spring of 2019. At present the plan is to transfer the krypton to the storage dewar during LS2 once the purity of the krypton has been measured and qualified.

No major detector upgrades are foreseen during LS2. A description of the detector can be found in [2]. A detector schematic is shown in Fig. 1, which displays the conventional sub-detector naming scheme used in this document. The major maintenance operation will concern the vacuum system. In particular, the cryo-pumps of the vacuum system will undergo a thorough check and key components will be replaced by an outside company. This will allow for efficient running of the vacuum system until LS3.

2.1 Trigger and DAQ

The NA62 TDAQ system is characterised by the need to sustain high level of data throughput from high rates in front-end electronics, without a clear $K^+ \rightarrow \pi^+ \nu \bar{\nu}$ signature at the trigger level.

The beam spill structure was much improved in 2018 with respect to the past but, because of the limited buffer size of the HPTDCs (high-performance TDC), the instantaneous rates to be handled by the readout electronics exceeded design specifications, despite running at an average intensity below nominal. Still, the infrastructure of the existing TDAQ system, including the hardware, proved to be robust and worked successfully at all intensities tested up to 100% of nominal.

It should be stressed that the system is very complex and a lot of effort was devoted to reduce the limitations of each sub-system. During the brief high-intensity period in 2018 we observed two issues in the firmware logic of the L0TP, one affecting the efficiency of some triggers for exotic processes, and one creating instability at 100% nominal intensity, which prevented us from maintaining such intensity for the rest of the data taking. Fixing the L0TP firmware is one of the major priorities in order to be able to run at 100% intensity after LS2. Studies are ongoing to resolve these issues and preliminary fixes, to be further tested in a realistic simulated environment, are already in place and we are confident both will be fully resolved in 2019.

The testing and eventual use of the system-wide L0 trigger back-pressure signal (CHOKe), present in the design since the start but not initially used, reduced the data taking losses due to beam non-uniformity to a tiny fraction of a burst, rather than an entire burst. Some unexpected hardware issues prevented the connection of all systems to this feedback network; however the successful use of CHOKe on some of the highest-rate sub-detectors had the effect that the whole TDAQ system benefited. The hardware problems will be fixed in 2019, allowing all systems to be connected to the CHOKe network, thus providing better handling of intensity spikes, which will minimize losses in future data taking.

The number of working spares for the common TDCB/TEL62-based system is about 5% of the total number of boards. All faults developed in the boards used in the beam were easily fixable. Most boards were produced around 2012, and several components are now obsolete and out of production. A pool of critical components was secured, to guarantee the possibility of repairs if the need arises. The availability of the (out of production) TEL62 daughter-cards, inherited from TELL1s, is secured, as a large number was procured after the dismantling of the readout of LHCb at the beginning of 2019. On top of this, the production of five more TEL62 and 10 more TDCBs is foreseen in 2019, and further components were acquired for this purpose.

The development of a FPGA-based TDC system, based on that created for the STRAW readout, and coupled to modern FELIX readout boards via GBT links, is ongoing. This system - with time resolution and channel packing suitable for the experiment - is expected to exhibit no rate limitations and to be insensitive to radiation. A prototype of this system was tested at the end of the 2018 run. For the post-LS2 data taking, two of the highest-rate sub-detectors (CHANTI and KTAG) will be equipped with this new readout system while the current system will be also maintained operational until the new readout is fully validated.

In conclusion, the readout and trigger system does not exhibit any major limitation and is suitable to be used in the next run period up to 100% intensity, including availability of a suitable number of spares.

The event building and data storage farm performed well in 2018, and will not need major changes during LS2. The same hardware infrastructure also hosts the execution of High-Level Trigger (HLT, as L1+L2) algorithms. The network was recently refurbished and the software is stable. The equipment will undergo routine maintenance, with the exchange of any components (e.g. disks or servers) upon failure. Benchmark testing during the short data taking period at 100% nominal intensity in 2018 revealed that, although it is possible to restart data taking with exactly the same trigger, the system could be subject to instabilities related to the spill structure. To improve the operation margin and increase the bandwidth, a multi-events packing mechanism in the LKr firmware readout will be implemented during LS2 and the DAQ chain will be re-evaluated prior to beam start. The same benchmarks have also indicated that there is still ample headroom in the computing power of the servers and so it is possible to introduce new software algorithms or refine the existing ones. Small upgrades to existing L1 triggers were performed in 2018. The time window for the L1 LAV was tuned to reduce possible random signal veto, while still ensuring enough reduction power. Dedicated versions of the L1 STRAW algorithm were implemented, aiming at: identifying decay channels with at least 3 reconstructed tracks in the final state; identifying vertices displaced from the nominal beam line due to long-

lived particles generated at the target or TAX. During LS2 we plan to: exploit correlations between subsystems at L2; exploit the information at L1 on position, time, energy given by the LKr calorimeter trigger; optimise the current L1 LAV trigger.

2.2 Sub-Detectors

The detector generally performed well in 2018. The following sub-detectors do not require interventions beyond maintenance: KTAG, CHANTI, STRAW, RICH, CHOD, NA48-CHOD, IRC, MUV1-2-3, SAC. Spares of front-end electronic and detector components are available. Maintenance includes: the replacement of CHANTI aging SiPM; the recovery of dead/noisy channels in KTAG and LAVs; the installation of the LAV internal calibration system in summer 2019, allowing to monitor the detector without beam during LS2; the refurbishment of the shaper boards in MUV1,2 and replacement of ageing photo-multipliers in MUV2; the replacement of the four RICH HV mainframes since maintenance is no longer guaranteed by the manufacturer and no spare mainframe is available. The RICH Neon quality is routinely monitored and it will be kept as it is until the start of data taking in 2021; one full neon fill is anyway already available.

Based on the experience of running the GTK, we foresee the need for 6 detector modules per year (3 in the beam + 3 spare). Taking into account some contingency in fabrication and operation, we aim at fabricating 15 new modules to cover data taking after LS2. Orders for all required parts have been placed. Assuming a fabrication rate of six detector modules per year, the modules and spares for future data taking periods should be secured by the end of 2019 and the whole production be completed by the end of 2021. The single hit time resolution was measured to be between 130 and 150 ps, and the full chain detection efficiency was around 97% per module.

No hardware problem affected the LKr CREAM readout in 2018; there were only a minimal number of faults, mainly in the VME power supplies. Some features of the firmware of the calorimeter readout system have been identified and will be discussed with the manufacturer for future improvement (see Section 3). As part of the maintenance, we plan to implement protection of the cooling pipes for the CREAM crates to avoid even minimal water drops inside the power supplies, and to find a viable solution for the vacuum leaks at the HV feedthroughs. Spares are available for all parts of the calorimeter's read out.

The HASC has also been proven to be effective as photon veto complementary to LAV, LKr, IRC and SAC calorimeters, with an additional 30% background reduction obtained in the analysis of 2016 Data. Given the success of the HASC as photon veto (also confirmed for the 2017 data), we plan to duplicate it in a position symmetrical with respect to the beam axis, to further increase the π^0 rejection.

3 Data: Preparation, Processing, Quality

The physics-grade 2018 data taking started just after an initial phase of about 10 days, dedicated to the setup and detector tuning. In total, 529191 physics-grade bursts were collected, corresponding to a total number of about 4×10^{12} Kaon decays recorded. A total of 388530 bursts were taken with the Fixed Collimator installed, while the other 140661 bursts were collected in the data taking period preceding the collimator installation, with conditions similar to 2017.

In addition to the traditional online monitor, a new system to further check the quality of the collected data was installed for the 2018 data taking. Control triggers from all the bursts collected were processed immediately after the writing to disk and a check was made for common failures that had been identified during the 2017 data taking; this enabled prompt detection of issues, particularly in the CREAM modules that are used to readout the LKr, MUV1 and MUV2

sub-detectors. All the issues detected could be fixed either performing a reset or reloading the firmware of the affected module(s) and, with the new system, the shift crew was immediately alerted to do so. Typically, issues of this kind were detected every 1-2 days of data taking and they were fixed in about 1-2 minutes from their occurrence.

Several essential improvements on the reconstruction and analysis software were implemented last year.

- Thanks to the development of an automatic time alignment procedure on a per-burst basis for all the crucial timing sub-detectors (KTAG, RICH, GTK), the detector synchronisation accuracy has been greatly improved.
- All the fine calibration constants (e.g. the LKr Energy scale, the GTK and STRAW momentum scale, the GTK alignment corrections) are now evaluated automatically on a per-run basis during processing and are available for user analyses.
- A file-based Condition Database (CDB) was introduced to have all the constants needed for calibration in a consistent scheme, and a Condition Service class was implemented to make the CDB easily accessible for all software uses (reconstruction, analysis, simulation).
- The existing software for bad burst detection was fine-tuned, in order to increase the failure detection efficiency and at the same time to reduce the amount of false positives.

The progress mentioned above on the software used for the data processing has led to the first processed 2017 and 2018 data samples with physics-grade performance. The current state-of-the-art calibration can now be obtained automatically from the central processing, without the need of any manual intervention or fine-tuning. The full 2017 data set has been processed with the newest software release and is available for physics analysis, as well as the high intensity (100% nominal) data sample taken at the end of the 2018 period. The processing of the other 2018 data samples has started, prioritizing the data collected after the installation of the Fixed Collimator. Also the 2016 data were re-processed with the newest software release. All the processed and filtered data are available on EOS for physics analysis. The full 2016–2018 sample is expected to occupy nearly 4 PBytes of space. We are currently preparing a high-level data format which will allow us to proceed towards an additional data reduction scheme, to simplify the data handling for the analysis step.

Thanks to the excellent performance of the LKr as a photon veto, the π^0 rejection inefficiency is currently at a level ($\sim 10^{-8}$) which is satisfactory for the physics analysis. Nevertheless, as already mentioned, specific data quality issues were discovered in the LKr data after the 2017 data taking, for the majority of which an offline correction procedure has already been developed. As already mentioned, all these issues can be cured online by a reset or a firmware reload, hinting at a CREAM firmware problem. We are currently interacting with CAEN, the external provider of the CREAM modules, with the goal of having the firmware fixed for the next data taking period after LS2. The progress towards addressing these issues would allow to tightening of the timing cuts at the analysis level and reduce the losses due to accidental activities 4.1.

4 $K^+ \rightarrow \pi^+ \nu \bar{\nu}$ Analysis

The $K^+ \rightarrow \pi^+ \nu \bar{\nu}$ analysis (later denoted as $\pi\nu\nu$) presented here has been performed on the full 2017 data sample, and it follows similar steps to the 2016 analysis published recently [1]. Beam fluctuations have been reduced in 2017, making it possible to run at an average intensity of 50–60%.

Data for $\pi\nu\nu$ have been collected with a two-level trigger stream (PNN). A hardware-based trigger (L0) used RICH, CHOD, LKr and MUV3 to veto μ^+ and γ while keeping π^+ . A

software-based trigger (L1) exploited K^+ identification with KTAG, γ rejection with LAV and track reconstruction with STRAW. The analysis makes also use of data taken with a downscaled minimum-bias trigger (control trigger) to compute the number of K^+ decays and to select control samples.

Data collected in 2017 for $\pi\nu\nu$ have been reprocessed in 2018 using the final sets of detector calibrations in the reconstruction step and then filtered to produce a dedicated $\pi\nu\nu$ stream for analysis.

A blind procedure is being adopted for the 2017 $\pi\nu\nu$ analysis, with signal and control regions kept masked until the evaluation of expected signal and background is completed.

The $\pi\nu\nu$ analysis of 2017 data is cut-based. The branching ratio of $K^+ \rightarrow \pi^+\nu\bar{\nu}$ predicted by the SM is $BR(K^+ \rightarrow \pi^+\nu\bar{\nu}) = (0.84 \pm 0.10) \times 10^{-10}$ [3]. The goal of the present analysis is to surpass the current published sensitivity [4, 5]. The analysis is organized into: selection, evaluation of the single event sensitivity, and background estimation and validation.

4.1 $K^+ \rightarrow \pi^+\nu\bar{\nu}$ Selection and Performance

The $\pi\nu\nu$ selection proceeds through: definition of a K^+ decay with a charged particle in the final state; rejection of events with γ or any other activity in final state; π^+ identification; kinematic selection and definition of the signal regions.

Signals in RICH, CHOD and LKr associated to a good-quality STRAW track timestamp the π^+ with $\mathcal{O}(100)$ ps resolution. KTAG and GTK identify and trace the K^+ , respectively. The time coincidence between KTAG, GTK and RICH and the spatial association between STRAW and GTK tracks are the criteria to match the parent K^+ with the corresponding π^+ . The performance is comparable to the 2016 analysis: the K^+ mis-matching probability is $\mathcal{O}(2\%)$ and the K^+ identification efficiency about 75%. Cuts on the decay vertex position and on the π^+ direction, and veto of events with extra-activity in CHANTI and GTK, select K^+ decays occurring in a fiducial decay region defined as in the 2016 analysis.

The out-of-time activity in GTK provides a precise event-by-event estimate of the instantaneous beam intensity. Figure 2 (left) illustrates the distribution of this variable for all the selected $K^+ \rightarrow \mu^+\nu$ decays taken in 2017 with the control trigger. Data span over a wide range of intensity, extending well above the design value. The wide range of intensity and the amount of data collected in 2017 allows a thorough analysis in bins of intensity.

The photon rejection exploits the time coincidence between π^+ and signals in LAV, LKr, IRC and SAC. Compared to 2016, the 2017 analysis benefits from a better treatment of the pileup in IRC and SAC and from an improved LKr reconstruction. The photon rejection still employs veto timing windows in LKr extending up to several tens of ns, necessary to cope with remaining LKr time mis-reconstructions. Promising studies are on-going to reduce the LKr veto timing windows and to mitigate the corresponding signal loss due to the accidental activity. As in the 2016 analysis, a multiplicity rejection based on the detection of extra activity in NA48-CHOD, CHOD and LKr, segments in STRAW and signals in HASC and MUV0 complements the photon rejection and suppresses multi-body decays like $K^+ \rightarrow \pi^+\pi^+\pi^-$ and $K^+ \rightarrow \pi^+\pi^-e^+\nu$. Figure 2 (right) shows the amount of accidental signal loss induced by the photon and multiplicity rejection as a function of the intensity, measured on data using $K^+ \rightarrow \mu^+\nu$ decays. With the present veto criteria the signal loss in 2017 amounts to 37% on average, in agreement with the intensity scaling when compared to the 2016 result. The average rejection inefficiency for π^0 s from $K^+ \rightarrow \pi^+\pi^0$ decays measured on data is $(1.4 \pm 0.1) \times 10^{-8}$, about 40% lower than that for the 2016 data analysis. Figure 3 illustrates the dependency of the inefficiency on π^+ momentum (left) and intensity (right). The momentum dependence suggests a progressive loss of hermeticity for high energy photons travelling close to the beam pipe. The π^0 rejection efficiency, in contrast, does not depend on the intensity within the statistical uncertainty.

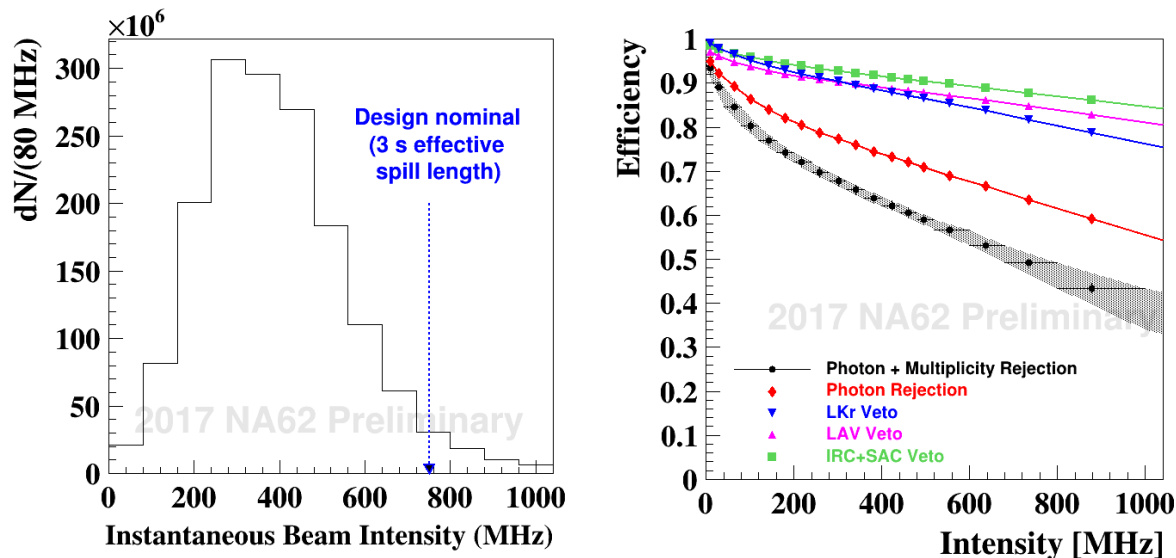


Figure 2: Left: distribution of the instantaneous intensity of selected $K^+ \rightarrow \mu^+\nu$ decays collected in 2017 using the control trigger; the value corresponding to the design nominal intensity at GTK3 under the assumption of 3 seconds effective spill length is also indicated for reference. Right: signal efficiency in bins of instantaneous beam intensity after photon and multiplicity rejection with total uncertainty, after photon rejection, after IRC and SAC veto only, after LAV veto only, after LKr veto only. Lines are guides for the eye.

A multi-variate classifier trained on 2016 data combines LKr, MUV1 and MUV2 information to provide π^+ identification. The RICH complements the calorimeters in particle identification. The 2017 analysis profits from a slightly improved usage of the RICH variables. The overall performance achieved is in agreement with that or better than those of the 2016 analysis (Fig. 4), suggesting that the higher beam intensity in 2017 has no significant effect on particle identification. Studies are on-going to improve the signal efficiency by further exploiting the correlations between RICH and calorimeters.

The invariant missing mass is $m_{miss}^2 \equiv (p_{K^+} - p_{\pi^+})^2$, with p_{K^+} (p_{π^+}) being the K^+ (π^+) 4-momenta measured by the GTK (STRAW). The m_{miss}^2 allows a kinematical separation between signal and background, in particular $K^+ \rightarrow \pi^+\pi^0(\gamma)$, $K^+ \rightarrow \mu^+\nu(\gamma)$ and $K^+ \rightarrow \pi^+\pi^+\pi^-$. Figure 5 shows the m_{miss}^2 as a function of π^+ momentum for the events passing the $\pi\nu\nu$ selection. Only events laying in the $K^+ \rightarrow \pi^+\pi^0$, $K^+ \rightarrow \mu^+\nu$ and $K^+ \rightarrow \pi^+\pi^+\pi^-$ background regions are shown. The $K^+ \rightarrow \pi^+\pi^0$ m_{miss}^2 peak has a resolution comparable to that measured in the 2016 data. Following the 2016 analysis approach, two signal regions are defined: the region at lower (higher) m_{miss}^2 is referred in the text as *region 1* (*2*). Signal regions are restricted to the (15, 35) GeV/c π^+ momentum band, as a compromise between signal acceptance and performance of π^0 detection and particle identification. In addition to the two signal regions, three control regions are defined to validate the $K^+ \rightarrow \pi^+\pi^0(\gamma)$ and $K^+ \rightarrow \mu^+\nu(\gamma)$ background estimates. Further kinematical constraints already employed in the 2016 analysis provide additional power to suppress background coming from tracks mis-reconstructed in STRAW or GTK. Both signal and control regions are kept masked in the 2017 analysis so far. In addition the region below the $K^+ \rightarrow \mu^+\nu$ decay is also masked, as will be used to validate the on-going studies of a possible background coming from the upstream beam line, called "upstream background".

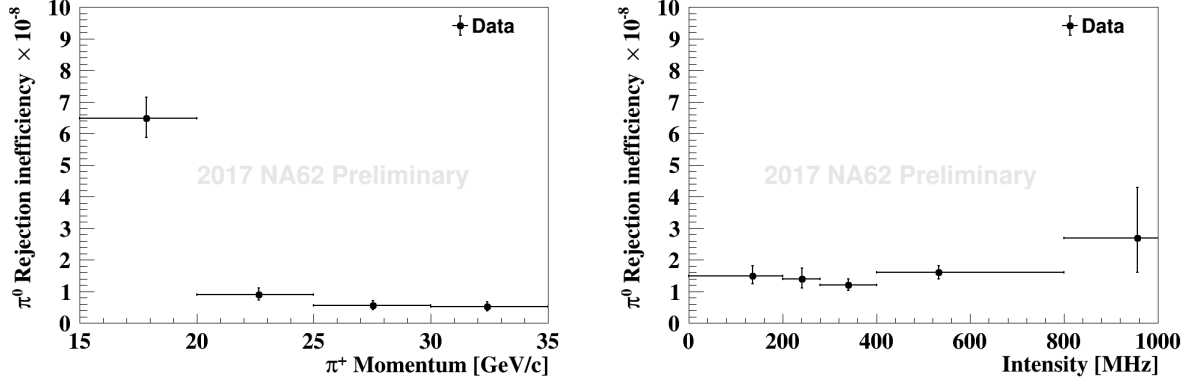


Figure 3: π^0 rejection inefficiency in bins of π^+ momentum (left) and of beam intensity (right) measured from data.

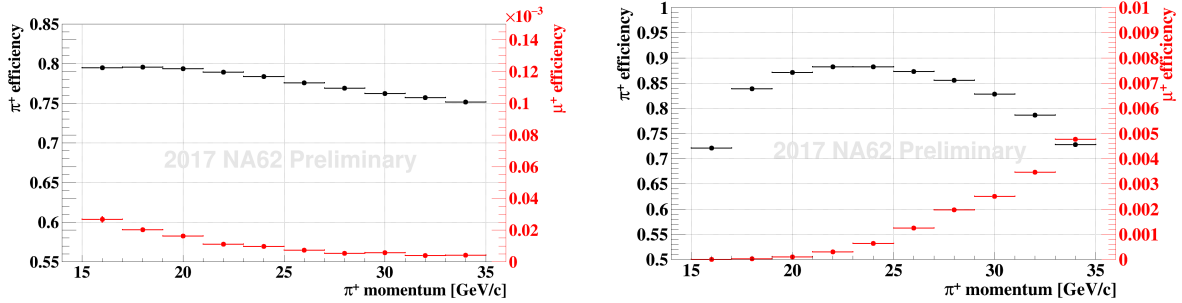


Figure 4: π^+ and μ^+ selection efficiency after applying particle identification criteria with calorimeters (left) and RICH (right).

Regions outside the fiducial π^+ momentum region are kept masked as sensitive to signal, even if with reduced sensitivity.

4.2 $K^+ \rightarrow \pi^+ \nu \bar{\nu}$ Single Event Sensitivity

The single event sensitivity is defined as $SES = 1/(N_K \cdot \varepsilon_{\pi\nu\nu})$, where N_K is the number of K^+ decays and $\varepsilon_{\pi\nu\nu}$ is the signal efficiency for the $\pi\nu\nu$ selection.

The measurement of N_K employs a sample of $K^+ \rightarrow \pi^+ \pi^0$ decays selected on control data using criteria similar to $\pi\nu\nu$, except photon and multiplicity rejection and kinematical cuts.

The following quantities contribute to $\varepsilon_{\pi\nu\nu}$: the signal acceptance extracted from Monte Carlo simulation, which is about 4% including also signal losses for particle identification; the signal efficiency for accidental losses due to photon and multiplicity rejection discussed previously, also called random veto efficiency; the PNN trigger efficiency, measured in data, varying between 85% and 90% and depending on π^+ momentum. The L0 trigger conditions on MUV3 and LKr mostly contribute to the PNN trigger efficiency. The L1 trigger is about 97% efficient, with losses due to the L1 LAV conditions. Correlation effects between trigger and random veto efficiency are under study.

Other effects reducing the signal acceptance not fully accounted for by the simulation, like

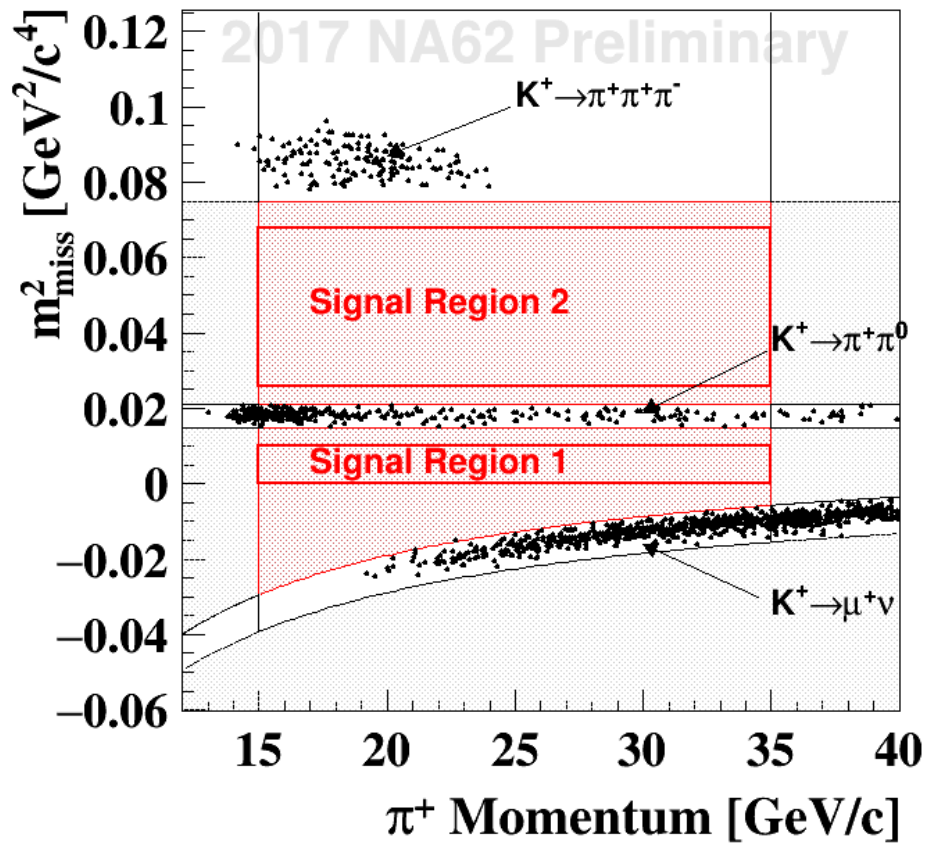


Figure 5: m_{miss}^2 as a function of π^+ momentum of the events in background regions passing the $\pi\nu\nu$ selection. Shaded area indicates the regions kept masked.

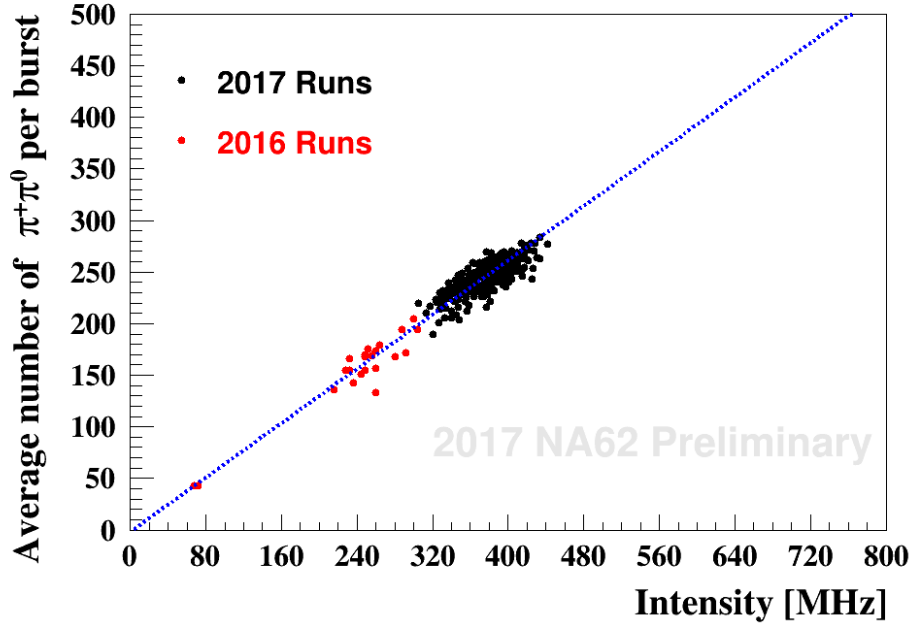


Figure 6: Average number of $K^+ \rightarrow \pi^+\pi^0$ decays per burst selected for normalization in some of the 2016 and 2017 runs as a function of the corresponding average beam intensity. The design nominal beam intensity is 750 MHz at GTK3 (under the assumption of 3 s effective spill length).

global detector efficiency or accidental losses due to muon rejection, cancel in the ratio between signal and normalization.

The SM $K^+ \rightarrow \pi^+\nu\bar{\nu}$ branching ratio allows the conversion of SES into the expected number of SM signal events. Table 1 summarizes the results of the 2017 data sensitivity. All the numbers are preliminary. Uncertainties are mostly systematic and conservatively reflect the uncertainties in the simulation.

N_K	$(13 \pm 1) \times 10^{11}$
SES	$(0.34 \pm 0.04) \times 10^{-10}$
Expected SM $K^+ \rightarrow \pi^+\nu\bar{\nu}$	2.5 ± 0.4

Table 1: Number of K^+ decays, N_K ; single event sensitivity, SES ; number of Standard Model signal events expected from the 2017 data analysis.

The overall 2017 single event sensitivity is about 10 times higher than that of 2016 data. The average number of $K^+ \rightarrow \pi^+\pi^0$ decays selected per burst scales linearly with the average burst intensity, even compared to the 2016 analysis (Fig. 6). This shows that the SES also scales linearly with the intensity, suggesting no additional losses with increasing intensity other than those expected from the random veto.

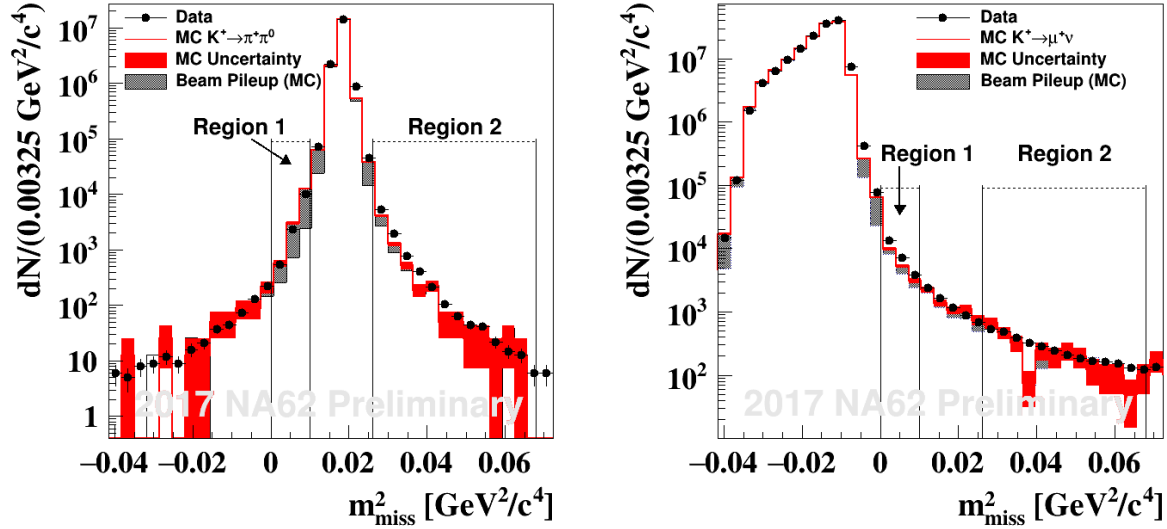


Figure 7: Distributions of the m_{miss}^2 of $K^+ \rightarrow \pi^+\pi^0$ (left) and $K^+ \rightarrow \mu^+\nu$ (right) events used to measure the tails of m_{miss}^2 . Monte Carlo prediction is also shown. The solid red bands indicate the 1σ systematic uncertainty of the Monte Carlo. The dark shadow bands illustrate the contribution of the beam pileup to m_{miss}^2 tails, as predicted from simulation.

4.3 Background Studies

The $K^+ \rightarrow \pi^+\pi^0(\gamma)$, $K^+ \rightarrow \mu^+\nu(\gamma)$, $K^+ \rightarrow \pi^+\pi^+\pi^-$ and $K^+ \rightarrow \pi^+\pi^-e^+\nu$ processes are the major sources of background from K^+ decays.

Sharp kinematic thresholds limit the m_{miss}^2 spectrum of $K^+ \rightarrow \pi^+\pi^0$, $K^+ \rightarrow \mu^+\nu$ and $K^+ \rightarrow \pi^+\pi^+\pi^-$, hence only m_{miss}^2 mis-reconstructions can cause these decays to enter the signal regions. The estimate of these backgrounds follows the lines of the 2016 data analysis. The procedure relies on the assumption that the cuts defining the signal regions are independent of π^0 rejection, particle identification and multiplicity rejection applied to suppress $K^+ \rightarrow \pi^+\pi^0$, $K^+ \rightarrow \mu^+\nu$ and $K^+ \rightarrow \pi^+\pi^+\pi^-$, respectively. As a consequence, the number of expected events in signal regions from each of the above processes, $N_{background}^{exp}$, is $N(background) \cdot f^{kin}$. Here $N(background)$ is the number of PNN triggered events in the corresponding background region surviving the $\pi\nu\nu$ selection, but the cut on m_{miss}^2 ; f^{kin} , called “tails”, is the fraction of background events entering signal regions because of m_{miss}^2 mis-reconstruction. The number $N(background)$ comes from a direct counting of the events in figure 5 for the three backgrounds mentioned above. Control samples properly selected on data allow the modelling of the tails and therefore the evaluation of f^{kin} . In addition to what was done for the 2016 data analysis, the study of f^{kin} on the 2017 data also includes studies of possible intensity-related effects.

A sample of $K^+ \rightarrow \pi^+\pi^0$ decays selected on control data tagging the π^0 with two γ 's in the LKr provides the model for the tails of the $K^+ \rightarrow \pi^+\pi^0$ m_{miss}^2 . Figure 7 (left) illustrates the distribution of the m_{miss}^2 of $K^+ \rightarrow \pi^+\pi^0$ events. Simulation agrees with data over 5 orders of magnitude within the statistical uncertainty, once the effect of the beam pileup is included. Figure 8 (top) display the size of the measured tails in bins of π^+ momentum (left) and beam intensity (right). These results show that 60%(20%) of the tails in region 1 (region 2) come from m_{miss}^2 mis-reconstruction due to $K^+-\pi^+$ mis-matching. This effect induces a slight dependence of f^{kin} on the intensity, confirmed by the simulation. Studies are on-going to improve the

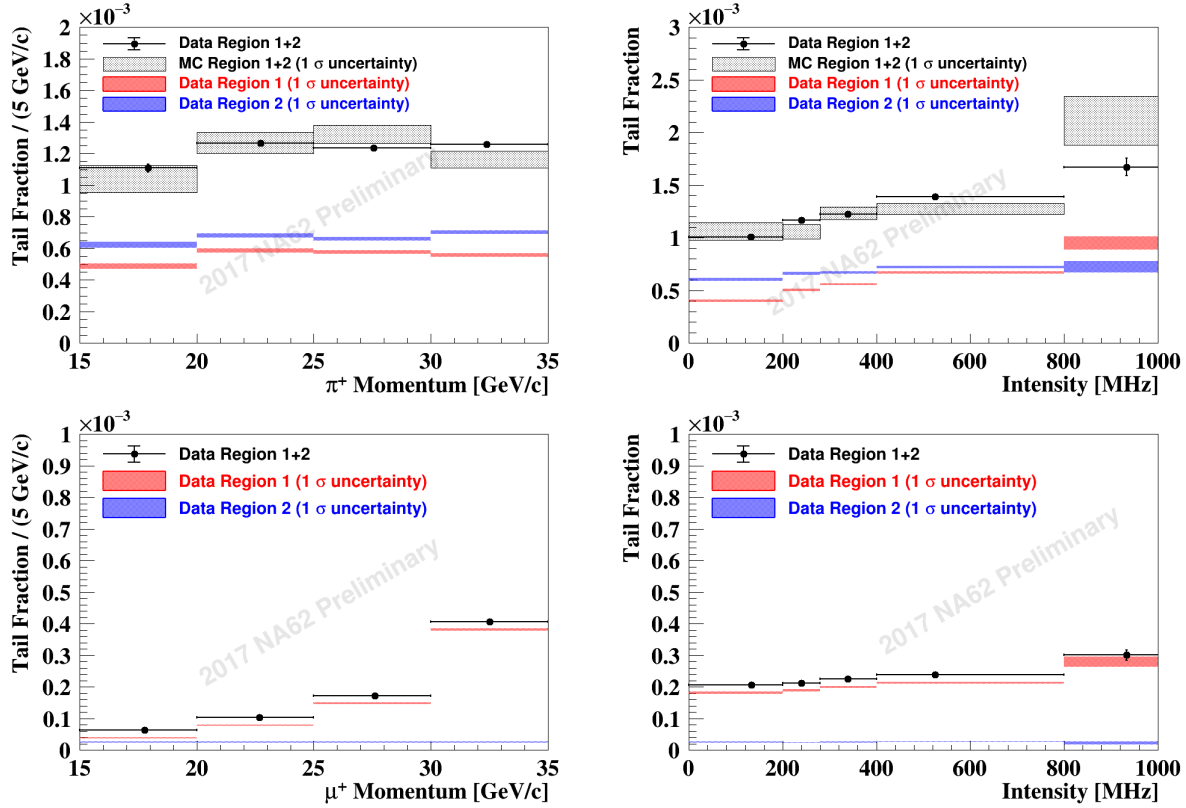


Figure 8: Fraction of $K^+ \rightarrow \pi^+\pi^0$ (top) and $K^+ \rightarrow \mu^+\nu$ (bottom) events entering regions 1 and 2 in bins of momentum (left) and intensity (right). Dots are data summed up in region 1 and 2. Red and blue boxes are data plotted separately for region 1 and 2, respectively. Grey shaded display the prediction from Monte Carlo simulation. The size of the boxes corresponds to 1σ statistical uncertainty.

algorithm for $K^+-\pi^+$ matching to reduce the tails further. The remaining part of f^{kin} is a consequence of the tracking material causing a significant deviation of the particle trajectory, thus largely irreducible. The selection criteria of the $K^+ \rightarrow \pi^+\pi^0$ do not bias the effects of mis-measurement on the m_{miss}^2 , but suppress the effect of additional radiative photons. Because the photon radiation causes m_{miss}^2 to enter region 2, it significantly decreases the kinematic rejection power and the background from radiative $K^+ \rightarrow \pi^+\pi^0$ needs a separate estimate. To this extent Monte Carlo studies show that the presence of the radiative photon increases by a factor 30 the suppression power of the photon rejection with respect to the non-radiative $K^+ \rightarrow \pi^+\pi^0$ decay. This feature overcompensates for the loss of kinematic rejection power and therefore the contribution from radiative $K^+ \rightarrow \pi^+\pi^0$ is an order of magnitude smaller than for the non-radiative case.

A sample of $K^+ \rightarrow \mu^+\nu$ selected by tagging the μ^+ with MUV3 signals provides the model for the tails of the $K^+ \rightarrow \mu^+\nu$ m_{miss}^2 (Fig 7, right). The fraction of $K^+ \rightarrow \mu^+\nu$ events entering region 1 is strongly dependent on the μ^+ momentum for kinematical reasons (Fig. 8, bottom left). Unlike the $K^+ \rightarrow \pi^+\pi^0$ background, the $K^+-\pi^+$ mis-matching has a minor impact on f^{kin} . The tails, therefore, do not show significant dependence on the intensity (Fig. 8, bottom right). The $K^+ \rightarrow \mu^+\nu$ control sample also includes the contribution from $K^+ \rightarrow \mu^+\nu(\gamma)$, which results in f^{kin} of the order of 10^{-5} in region 2.

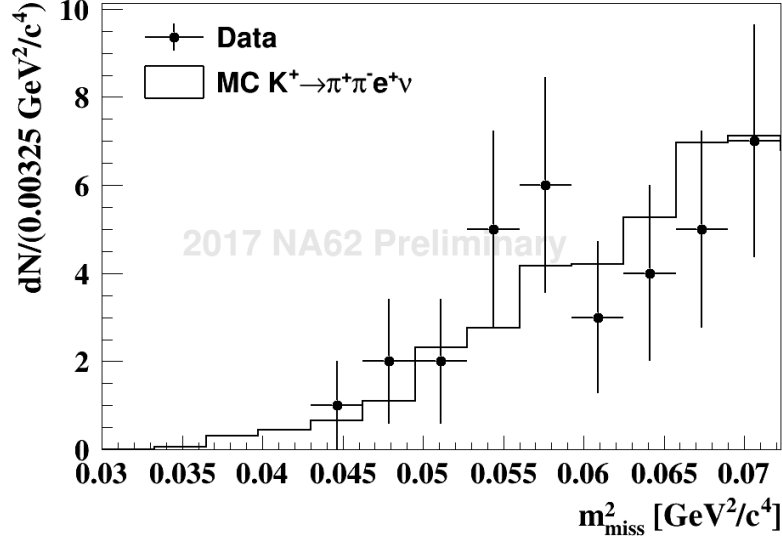


Figure 9: m_{miss}^2 of a $K^+ \rightarrow \pi^+\pi^-e^+\nu$ enriched sample of events used to validate the $K^+ \rightarrow \pi^+\pi^-e^+\nu$ Monte Carlo simulation. Dots are data, solid histogram Monte Carlo.

The number of residual events in the $K^+ \rightarrow \pi^+\pi^+\pi^-$ region clearly indicates that the suppression power of the multiplicity rejection is comparable to that achieved in 2016. m_{miss}^2 tails are presently under evaluation. Nevertheless the studies on the kinematic tails mentioned above already suggest that the higher intensity is expected to have a minor, if not negligible, impact.

The same argument of $K^+ \rightarrow \pi^+\pi^+\pi^-$ applies to $K^+ \rightarrow \pi^+\pi^-e^+\nu$ background, whose suppression critically relies on the multiplicity rejection. The estimate of this background makes use of simulation because kinematics and topology are strongly correlated in $K^+ \rightarrow \pi^+\pi^-e^+\nu$ decays. The 2017 data analysis profits of a Monte Carlo sample of about 1.5×10^9 decays, a factor four larger than that used in the 2016 analysis. $K^+ \rightarrow \pi^+\pi^-e^+\nu$ enriched samples selected by inverting some of the multiplicity criteria allow for a statistically significant validation of the simulation with data (Fig. 9).

The photon rejection and particle identification performance achieved in 2017 make the backgrounds from $K^+ \rightarrow e^+\pi^0\nu$, $K^+ \rightarrow \mu^+\pi^0\nu$ and $K^+ \rightarrow \pi^+\gamma\gamma$ negligible, as in 2016.

In addition to K^+ decays in the fiducial region, backgrounds can originate from upstream events. The studies of these backgrounds are still ongoing.

Table 2 summarizes the expected background from kaon decays in signal region 1 and 2. Studies in bins of intensity have shown that the signal-over-background ratio is largely independent from the intensity, within the statistical uncertainty.

The understanding of the background processes achieved so far through the analysis of the 2017 data allows a detailed comparison of data and background models of the m_{miss}^2 . This is illustrated in Figure 10.

The m_{miss}^2 distributions for $K^+ \rightarrow \pi^+\pi^0$, $K^+ \rightarrow \mu^+\nu$ and $K^+ \rightarrow \pi^+\pi^+\pi^-$ come from control data. These distributions are normalized separately to the number of events remaining in the corresponding background regions after the $\pi\nu\nu$ selection. The simulation provides the modelling for the radiative $K^+ \rightarrow \pi^+\pi^0$ decay. $K^+ \rightarrow \pi^+\pi^-e^+\nu$ background comes from simulation after relaxing some of the multiplicity conditions and it is normalised to the expected number of $K^+ \rightarrow \pi^+\pi^-e^+\nu$ events in signal region. The full kinematic constraints defining regions 1 and

Process	Expected events in signal regions
$K^+ \rightarrow \pi^+\pi^0(\gamma)$ IB	$0.35 \pm 0.02_{stat} \pm 0.03_{syst}$
$K^+ \rightarrow \mu^+\nu(\gamma)$ IB	$0.16 \pm 0.01_{stat} \pm 0.05_{syst}$
$K^+ \rightarrow \pi^+\pi^-e^+\nu$	$0.22 \pm 0.08_{stat}$
$K^+ \rightarrow \pi^+\pi^+\pi^-$	$0.015 \pm 0.008_{stat} \pm 0.015_{syst}$
$K^+ \rightarrow \pi^+\gamma\gamma$	$0.005 \pm 0.005_{syst}$
$K^+ \rightarrow l^+\pi^0\nu_l$	$0.012 \pm 0.012_{syst}$
Upstream Background	Analysis on-going

Table 2: Summary of the background integrated in region 1 and 2, as estimated from the preliminary $\pi\nu\nu$ analysis of 2017 data. Systematic uncertainties are taken conservatively from the 2016 analysis. $K^+ \rightarrow \pi^+\pi^0$ includes also the radiative component which accounts for about 10% of the total background.

2 are applied in Figure 10 and give rise to the wrinkled $K^+ \rightarrow \pi^+\nu\bar{\nu}$ m_{miss}^2 shape around the edges of the signal regions. The signal is normalised to the 2017 expected numbers of Standard Model $K^+ \rightarrow \pi^+\nu\bar{\nu}$ events in regions 1 and 2. The contribution from the upstream background is missing. The remarkable agreement between the shape of the modelled m_{miss}^2 and that of the data remaining in the background regions confirms the validity of the factorisation approach used to evaluate the background from the main K^+ decay modes. Figure 11 shows the same m_{miss}^2 distribution separated into four π^+ momentum bins. The above figures show that the shapes of the m_{miss}^2 differ substantially between signal and background in signal regions and strongly depend on π^+ momentum. Studies are on-going to make use of this feature in order to enhance the sensitivity for a given signal-over-background ratio with respect to a simple counting analysis.

4.4 Summary and Prospects

With a lower background level than that in 2016 and an expectation of $O(3)$ SM $K^+ \rightarrow \pi^+\nu\bar{\nu}$ events, we foresee a publication in 2019 surpassing the E787/E949 sensitivity. We have demonstrated that the signal-over-background ratio for $K^+ \rightarrow \pi^+\nu\bar{\nu}$ does not deteriorate significantly when increasing the beam intensity. In addition to the efforts taken to improve the random veto, the analysis is focusing to decrease the background further. This will be used as a possible leverage to eventually relaxing some of the selection conditions to increase the signal acceptance. The estimate of the upstream background is ongoing. The precise evaluation of the total statistics collected in 2018 is under study. In any case further data taking is necessary to reach the proposed precision.

5 Rare and forbidden decays

A number of dedicated rare decay trigger chains have been in operation during the 2016–18 data taking. The multi-track L0 triggers for collection of K^+ decays to lepton pairs (i.e. di-muons, di-electrons and muon-electron pairs) are based on RICH and CHOD multiplicity requirements, as well as total LKr energy deposit and MUV3 signal multiplicity conditions. This is followed by beam kaon identification by the KTAG and reconstruction of a negatively charged track in

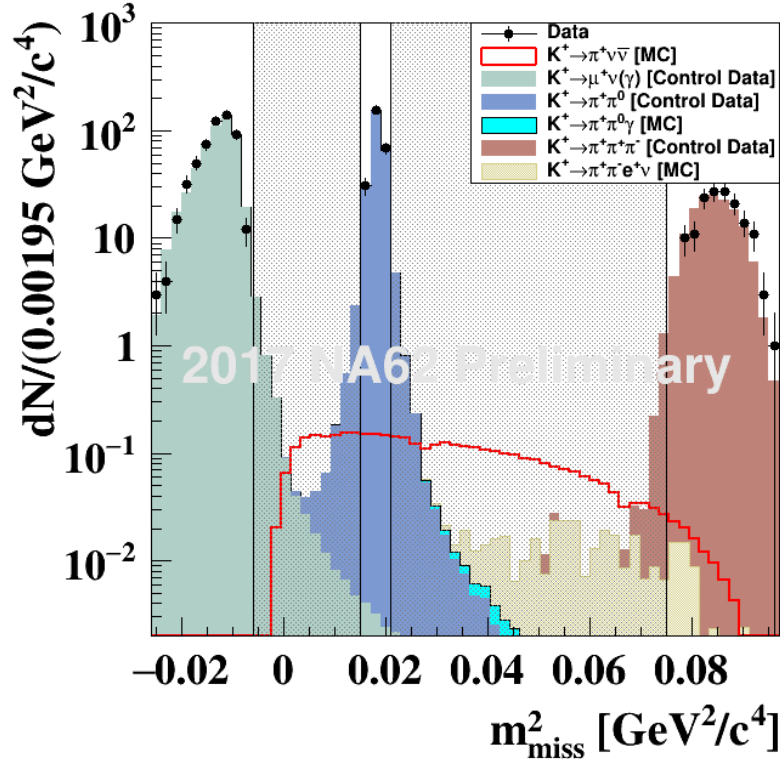


Figure 10: m_{miss}^2 integrated over π^+ momentum for signal and background, compared with the data remaining in background regions after the $\pi\nu\nu$ analysis. The signal (red histogram) is superimposed for comparison. Shaded bands comprise signal and control regions and are kept masked in the analysis.

the spectrometer at L1. The di-muon trigger is typically downscaled by a factor of 2, while the di-electron and muon-electron pair triggers are downscaled by factors up to 10. A generic multi-track trigger without particle identification (downscaled by $D = 100$) and a minimum bias control trigger based on hodoscope signals ($D = 400$) are also available.

Large data samples have been collected for rare decay measurements and searches for new physics. The large number of kaon decays collected is complemented by the excellent resolution on kinematic variables, particle identification and photon veto capabilities of the NA62 detector, leading to favourable background conditions. The available data set provides the potential for precision measurements of rare kaon decays [7], including $K^+ \rightarrow \pi^+ \mu^+ \mu^-$, $K^+ \rightarrow \pi^+ \gamma \gamma$, $K^+ \rightarrow e^+ \nu \gamma$, $K^+ \rightarrow \mu^+ \nu \gamma$, $K^+ \rightarrow \ell^+ \nu \mu^+ \mu^-$ ($\ell = e, \mu$), and $K^+ \rightarrow \pi^0 e \nu \gamma$. Physics beyond the SM is also being explored: searches for K^+ decays forbidden in the SM, resonances in multi-body K^+ decays (which can be interpreted in terms of dark vector, dark scalar or axion emission [8, 9, 10]), and heavy neutral lepton production [11] in K^+ decays are being performed at record levels of sensitivity.

A recent highlight from the rare decays working group, which illustrates the physics potential in terms of statistical precision and backgrounds, is the first result from the searches for lepton number violating decays $K^+ \rightarrow \pi^- e^+ e^+$ and $K^+ \rightarrow \pi^- \mu^+ \mu^+$ with the 2017 data. In the original Standard Model (SM), the neutrinos are strictly massless due to the absence of right-handed chiral states. The discovery of neutrino oscillations has conclusively demonstrated that neutrinos

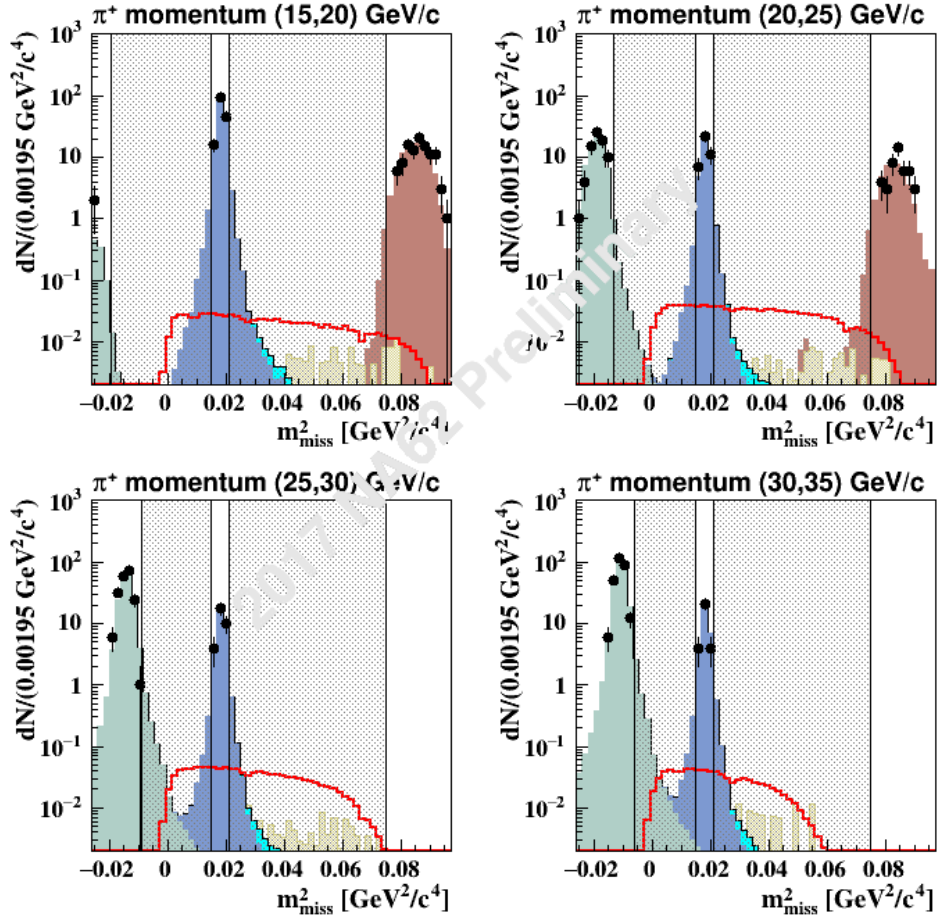


Figure 11: m_{miss}^2 in different π^+ momentum bins for signal and background. The same color code as of Figure 10 is used.

have non-zero masses, therefore calling for an extension of the SM. For a non-zero mass, it is possible in principle to distinguish experimentally between the Dirac and Majorana nature of the neutrino. Observation of a process violating lepton number by two units would provide a strong evidence for the Majorana nature of the neutrino, and the NA62 experiment is uniquely sensitive to the neutrinoless double beta decays of the charged kaon.

The data sample analysed corresponds to $2(8) \times 10^{11}$ kaon decays in the fiducial decay region for the $K^+ \rightarrow \pi^- e^+ e^+$ ($K^+ \rightarrow \pi^- \mu^+ \mu^+$) search. A blind analysis has been performed, and the following limits on the branching fractions of lepton number violating kaon decays have been obtained at 90% CL:

$$\begin{aligned} \mathcal{B}(K^+ \rightarrow \pi^- e^+ e^+) &< 2.2 \times 10^{-10}, \\ \mathcal{B}(K^+ \rightarrow \pi^- \mu^+ \mu^+) &< 4.2 \times 10^{-11}, \end{aligned}$$

improving over the world data [12, 13]. The reconstructed mass spectra obtained within the two analyses are shown in Fig. 12. The result is presented at the Moriond EW 2019 Conference. None of the searches is limited by background, and analysis of the full 2016–18 sample is expected to improve the sensitivity by a further factor of 3. Searches for other lepton number and lepton flavour violating decays with similar sensitivities are in progress, and further new results are expected in 2019.

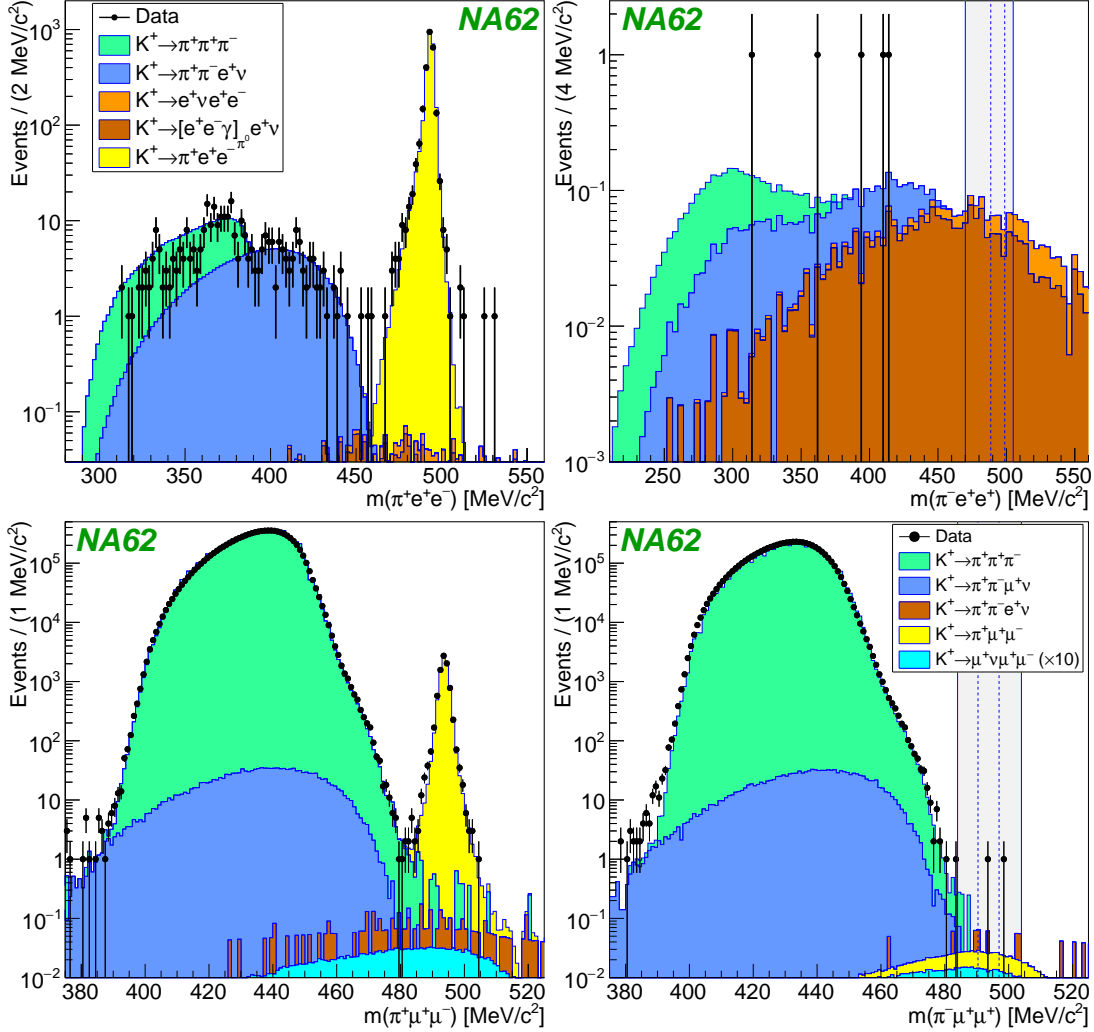


Figure 12: Illustration of the searches for lepton flavour and number violating K^+ decays with the 2017 data: reconstructed mass spectra of the $\pi^-e^+e^+$ (top right), $\pi^-\mu^+\mu^+$ (bottom right). The signal regions and the wider regions that were blinded during the analysis are indicated with the vertical bands. Illustration of the corresponding SM decay channels $\pi^+e^+e^-$ (top left), $\pi^+\mu^+\mu^-$ (bottom left) final states.

6 Exotic searches

One of the possible extensions of the SM aimed at explaining the abundance of dark matter in our universe predicts a new $U(1)$ gauge-symmetry sector, with a vector mediator field A' named as “dark photon”. In a simple realization of such a scenario [14, 15], the A' field would (feebly) interact with the SM photon through a “kinetic mixing” Lagrangian with a coupling parameter ϵ .

In a general picture, the kinetic mixing Lagrangian might be accompanied by further interactions, both with SM matter fields and with a secluded, hidden sector of possible dark-matter candidate fields. If these are lighter than the A' , the dark photon would decay mostly “invisibly,” so that a missing-energy signature might reveal its presence.

A search for an invisible dark photon A' has been performed. The NA62 photon-veto rejection, precisely studied in the context of the analyses for $K^+ \rightarrow \pi^+\nu\bar{\nu}$ and for the search for π^0 decays to invisible final states, is paramount for the A' search. The analysis has been performed with a fraction of the 2016 data, equivalent to $\approx 1\%$ of the total kaon flux collected by NA62

through 2018.

This search is performed by means of the decay chain $K^+ \rightarrow \pi^+\pi^0$ with $\pi^0 \rightarrow A'\gamma$, where, given the kaon, pion, and photon 4-momenta, the squared missing mass $M_{\text{miss}}^2 = (P_K - P_\pi - P_\gamma)^2$ is expected to peak around the squared A' mass for the signal and around zero for the dominant background due to $\pi^0 \rightarrow \gamma\gamma$ decays with one photon undetected. A peak search has been conducted, comparing signal-selected samples and data-driven background estimates.

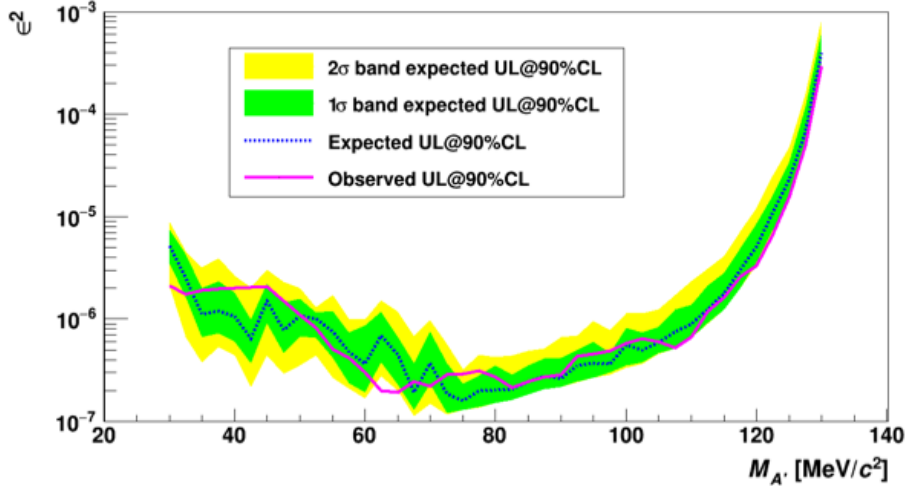


Figure 13: Upper limits at 90% CL on the dark photon coupling strength ϵ_z as a function of the mass $M_{A'}$. The limit obtained from data (solid line) should be compared to that expected in the absence of signal: the median of the upper-limit distribution in the background-only hypothesis is shown by the dashed line and the corresponding fluctuation bands with 68% and 95% coverage are shown by the shaded areas.

No significant statistical excess has been identified and upper limits on the coupling strength ϵ^2 in the mass range 30–130 MeV/c^2 have been set at the level between 2×10^{-6} and 2×10^{-7} , improving on the previous limits over the mass range 60–110 MeV/c^2 (Fig. 13). The result is final and supersedes the preliminary one presented in 2017. A paper has been submitted for publication (CERN-EP-2019-048) and the result is presented at the Moriond QCD 2019 Conference.

In addition, more general studies of sensitivity for long-lived states have been performed within the Physics Beyond Colliders BSM Working group. One nominal year of NA62 data taking at 100% intensity corresponds to few 10^{18} protons on T10 target (POT), which in turn correspond to 10^{18} mesons ($\pi^0, \eta, \eta', \Phi, \rho, \omega$) and 10^{15} (10^{12}) charmed (beauty) mesons. The mesons might decay to exotic particles (dark photons, heavy neutral leptons, etc.) which are expected to have feeble interactions with SM fields and therefore to be extremely long lived. An exotic particle (dark photons, heavy neutral leptons, dark scalars and axion-like particles) produced in the target might reach the NA62 sensitive volume, decaying therein. Details on the various new-physics models and the quantitative assumptions made are given in the BSM Working group report [16].

7 Publications of NA62 data and older data

Since the last NA62 SPSC review in April 2018, the collaboration has completed the following publication:

- E. Cortina Gil *et al.* (NA62 collab.), First search for $K^+ \rightarrow \pi^+ \nu \bar{\nu}$ using the decay-in-flight technique, Phys. Lett. B791 (2019) 156.

More analyses based on the 2003-2004 data of NA48/2 have been published:

- J. R. Batley *et al.* (NA48/2 collab.), First observation and study of the $K^\pm \rightarrow \pi^\pm \pi^0 e^+ e^-$ decay, Phys. Lett. B788 (2019) 552.
- J. R. Batley *et al.* (NA48/2 collab.), Measurement of the form factors of charged kaon semileptonic decays, JHEP 10 (2018) 150.

The collaboration is actively contributing to major International Conferences and topical Workshops with NA62 Detector contributions and recently published or preliminary physics results from NA62 and NA48/2 data analyses. In the past year (May 2018 to April 2019), the collaboration speakers presented 43 talks and 3 posters to Physics Conferences and 7 talks and 1 poster to Instrumentation Conferences. More contributions are already foreseen in future 2019 Conferences. Most notably, the highlights presented in the rare decays and in the exotic searches sections are presented at Moriond EW 2019 and Moriond QCD 2019 respectively.

References

- [1] E. Cortina Gil *et al.* (NA62 collab.), First search for $K^+ \rightarrow \pi^+ \nu \bar{\nu}$ using the decay-in-flight technique, Phys. Lett. B791 (2019) 156.
- [2] The NA62 Collaboration, JINST **12** (2017) P05025
- [3] A.J. Buras, D. Buttazzo, J. Girrbach-Noe and R. Knegjens, JHEP **1511** (2015) 33
- [4] A.V. Artamonov, *et al.*, Phys. Rev. Lett. 101 (2008) 191802.
- [5] A.V. Artamonov, *et al.*, Phys. Rev. D 79 (2008) 092004.
- [6] M. Tanabashi, *et al.* [Particle Data Group], Phys. Rev. D 98 (2018) 030001.
- [7] V. Cirigliano *et al.*, Rev. Mod. Phys. **84** (2012) 399.
- [8] F. Bezrukov and D. Gorbunov, JHEP **05** (2010) 010.
- [9] D. Alves and N. Weiner, JHEP **07** (2018) 092.
- [10] G. Krnjaic *et al.*, arXiv:1902.07715.
- [11] L. Canetti *et al.*, Phys. Rev. **D87** (2013) 093006.
- [12] R. Appel *et al.*, Phys. Rev. Lett. **85** (2000) 2877.
- [13] J.R. Batley *et al.*, Phys. Lett. **B796** (2017) 67.
- [14] L. Okun, Sov.Phys.JETP 56 (1982) 502.
- [15] B. Holdom, Phys.Lett. B166 (1986) 196.

- [16] J. Beacham *et al.*, “Physics Beyond Colliders at CERN: Beyond the Standard Model Working Group Report,” arXiv:1901.09966 [hep-ex].
- [17] J. P. Lees, et al. [The BaBar Collaboration], Phys. Rev. Lett. 119 (2017) 131804.
- [18] D. Banerjee, et al. [The NA64 Collaboration] Phys. Rev. D 97 (2018) 072002.
- [19] “Muon Anomalous Magnetic Moment”, within M. Tanabashi, et al. [Particle Data Group], Phys. Rev. D 98 (2018) 030001.
- [20] P. Fayet, Phys. Rev. D 75 (2007) 115017.
- [21] M. Pospelov, Phys. Rev. D 80 (2009) 095002.